

Novel approach to calculate electrical currents in stator-, field- and damper-windings at three-phase sudden short-circuit for large synchronous generators

M. Hackbart

In this manuscript the novel methodology of quick and accurate calculation of the rotor and stator currents during a three-phase sudden short-circuit is presented. The proposed approach consists of two parts. *First*, the detailed finite element model is developed. It accounts for stator core and winding, rotor yoke and winding, damper winding and conductive rotor surface. *Second*, the revised analytical formulation of the existing approaches to evaluate transient field current behavior during a three-phase sudden short-circuit is presented. Four phenomenological coefficients are introduced for proper representation of the field winding current. The developed methodology is feasible for solid and laminated rotors, with and without damper bars. It is demonstrated that there is good agreement between the results of our theoretical approach and the factory tests.

Keywords: finite element analysis; synchronous generator; three phase sudden short circuit

Neuartiger Ansatz zur Berechnung der elektrischen Ströme in der Ständer-, Erreger- und Dämpferwicklung beim dreiphasigen Stoßkurzschluss für große Turbogeneratoren.

Dieser Beitrag stellt eine mögliche Methodik vor, welche die Läufer- und Ständerströme im dreiphasigen Stoßkurzschluss von Turbogeneratoren großer Leistung bestimmt. Als erstes wird ein Finite-Elemente-Modell präsentiert, welches das Ständerblechpaket, die Ständerwicklung, das Rotorjoch, die Rotorwicklung und den Dämpferkreis abbildet. Im nächsten Schritt wird eine analytische Gleichung vorgestellt, die den Rotorstromverlauf mittels vier Koeffizienten beschreibt. Die analytische Gleichung kann die zeitveränderlichen Ströme im dreiphasigen Stoßkurzschluss für massive und geblechte Rotoren sowie mit und ohne Dämpferkreis beschreiben. Die analytische Gleichung wurde von den Ergebnissen des Finite-Elemente-Modells abgeleitet. Das Finite-Elemente-Modell und die analytische Beschreibung zeigen gute Übereinstimmung mit den im Prüffeldprobelauf gemessenen Strömen.

Schlüsselwörter: Finite-Elemente-Analyse; Turbogenerator; dreiphasiger Stoßkurzschluss

Received October 20, 2015, accepted January 29, 2016, published online March 3, 2016
© Springer Verlag Wien 2016



Nomenclature		T_d''	Sub-transient time constant
3P-SSC	Three-phase sudden short-circuit	T_d'	Transient time constant
f	Frequency	u_{fd}	Field winding voltage
FEA	Finite element analysis	$U_{L(a)}$	RMS stator voltage in phase (a)
i_f	Field current	X_d	Synchronous reactance
i_s	Stator current	X_d'	Transient reactance in d-axis
K_0, K_1, K_2, K_3	Coefficients for analytical description of rotor currents	X_d''	Sub-transient in d-axis direction
l_s	Length of stator end winding	X_q	Sub-transient reactance in q-axis direction
L_m	Mutual damper wedge and self-inductance	X_H	2D Finite element straight part main reactance (excluding end zone leakage, but include stator slot leakage)
L_s, X_s	Stator winding leakage inductance/reactance	X_f	2D Finite element rotor reactance (excluding end zone leakage)
R_1, R_2, \dots	Wedge to retaining ring contact resistors	λ_s	Permeance factor for end winding leakage reactance
R_a, R_b, \dots	Axial wedge resistance	ϑ_0	Phase angle ($0^\circ, +120^\circ, -120^\circ$)
R_K	Damper winding contact resistance		
R_A	Armature resistance		
R_f	Field winding resistance		
T_a	Armature time constant		
T_{dO}	Transient time constant when rotor surface is conductive		

Hackbart, Michael, Power and Gas Division, Large Gas Turbines, Generators, Siemens AG, Werner v. Siemens Straße 1, 99085 Erfurt, Deutschland
(E-mail: michael.hackbart@siemens.com)

w Number of stator winding turns in series for voltage induction
 $\omega = 2\pi f$ Angular frequency

1. Introduction

The stator and rotor currents of salient pole and round rotor machines have been discussed over the past several decades. The milestone “Two-Reaction Theory of Synchronous Machines” has been developed by R.H. Park almost 90 years ago [1]. Several studies have exploited this work as basis for description of performance of synchronous machines [2–8]. For example, the calculations “of Synchronous Machine Constants-Reactances and Time Constants Affecting Transient Characteristics” have been presented by L. Kilgore in 1931 [2]. Later on, Ch. Concordia developed the theory of performance of synchronous machines, which has been published in 1951 [3]. In the framework of his study, novel reactance and time constants, which became called sub-transient, transient and steady-state parameters of a synchronous machine, has been discussed.

Generator overall performance has been described in [3–8] using analytical equations and equivalent circuit parameters. Evaluation of generator parameters for sub-transient, transient and steady state operation has been performed with a three-phase sudden short-circuit (3P-SSC) test. The details of this procedure have been explained in [3–5]. Traditional mathematical models that simulate stator currents provide insufficient description of the field current behavior, and the discrepancies between measurements and calculations have been revealed. The work of Canay [9] has introduced detailed models of equivalent circuits that help to correctly represent field current behavior.

To further refine existing industry’s approaches to the involved phenomena, non-linear transient finite element methodology has been developed in [10–13]. Effects caused by leakage have been discussed in [14–17]. Non-linear transient FEA gives deeper insight into electromagnetic processes in the generator and helps one to derive transients in the stator-, field-, damper windings and on the rotor surface. More information about methods and approaches to evaluation of electrical parameters of synchronous machines can be found in [18–23].

Application of non-linear FEA for controlling and calculation of the transient currents in the windings for an arbitrary electrical machine is very time-consuming. On the other hand, the existing analytical approaches to evaluation of the rotor current behavior are too oversimplified in order to provide a proper description of the investigated phenomena. In this manuscript a novel methodology of quick and accurate calculation of the rotor and stator currents at 3P-SSC in large synchronous generators is presented. This approach combines finite-element and analytical studies. The detailed finite element model, which involves all crucial elements of a synchronous electrical machine (namely stator core and stator winding, rotor yoke and rotor winding, damper winding and conductive rotor surface), is presented. The new analytical approach to describe time-dependent field winding current at 3P-SSC event, based on the results of the FEA, is developed. Our studies give clear evidence that our approach is feasible for both, solid and laminated rotors, with and without damper bars. The phenomenological coefficients in the developed equation are revealed to be unique for a certain type of an electrical machine and can be exploited for other generators of this type without limitations.

2. State-of-the-art analytical description of the three phase sudden short circuit

In this section the state of the art analytical description of the 3P-SSC is discussed.

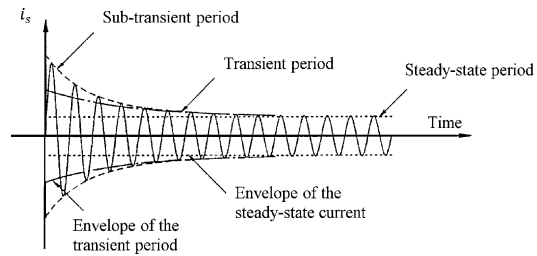


Fig. 1. Stator current at 3P-SSC

Generator parameters for transient, sub-transient and steady state operation are derived in [3, 4] and [5] from stator current analysis. Figure 1 shows 3P-SSC event, which is divided in three periods: sub-transient, transient and steady state ones.

The electrical time constant of the damper winding is significantly smaller than that of the field winding. It promotes faster decay of currents induced in the damper winding than that induced in the field winding. Typical time constants for the damper winding lie between 20 and 50 ms (sub-transient period, Fig. 1), while field winding time constants—between 0.5 and 2 s (transient period, Fig. 1). In the following this transient period is denoted with the prime (') and the sub-transient period—with double prime (") as indices. Stator current at 3P-SSC is approximated as follows [4]:

$$i_s = -\sqrt{2}U_{L(a)} \left\{ \left[\frac{1}{X_d} + \left(\frac{1}{X_d'} - \frac{1}{X_d} \right) e^{-\frac{t}{T_d'}} + \left(\frac{1}{X_d''} - \frac{1}{X_d'} \right) e^{-\frac{t}{T_d''}} \right] \times \cos(\omega t + \vartheta_0) + \frac{1}{2} \left[\frac{1}{X_d''} + \frac{1}{X_q''} \right] e^{-\frac{t}{T_a}} \cos(\vartheta_0) + \frac{1}{2} \left[\frac{1}{X_d''} - \frac{1}{X_q''} \right] e^{-\frac{t}{T_a}} \cos(2\omega t + \vartheta_0) \right\} \quad (1)$$

Equation (1) describes the current time functions in all 3 phases. Relations between the three phases are given with $\vartheta_0 = 0, 120^\circ$ and -120° . X_d'' and X_q'' are sub-transient reactances in d- and q-axes, X_d' is transient reactance and X_d is synchronous reactance. The armature time constant T_a depends on the armature resistance R_a . The transient period time constant is T_d' and the sub-transient period time constant is T_d'' . Saturation effects are represented by introducing normal, half and saturated values for transient and sub-transient reactances.

Field current behavior at 3P-SSC can be analytically calculated by means of Eq. (2) [4]:

$$i_f(t) = I_{f0} \left[1 + \left(\frac{X_d}{X_d'} - 1 \right) e^{-\frac{t}{T_d'}} - \left(\frac{X_d}{X_d''} - 1 \right) e^{-\frac{t}{T_a}} \cos(\omega t) \right] \quad (2)$$

Here I_{f0} is the field current before the 3P-SSC is initiated. This equation includes transient and armature time constants, as well as transient and synchronous reactances. Sub-transient time constant and reactance are not part of the equation; they are associated with the damper circuit. As it will be shown in Sect. 4 (scenario 1), the Eq. (2) is valid for machines without damper circuit and with non-conductive rotor surface.

3. Novel approach: finite element model

In this section the non-linear transient finite element model, which is developed in the framework of our investigation and accounts for stator, rotor and damper windings, is presented and discussed.

3.1 Model description

The 2-pole generator that is examined with 2D finite element method has the apparent power of 370 MVA and terminal voltage

of 20 kV. The 3P-SSC that is studied is initiated from open circuit condition at 70 % terminal voltage. Figure 2 shows the stator core (A), stator winding (B), rotor yoke (C), damper bars (D) and field winding (E) as they are represented in the finite element model. The rotor diameter is ~1.2 m, the stator core outer diameter is ~3 m, and the generator length is 5.5 m.

The exploited mesh is presented in Fig. 2 and its details are shown in Fig. 3. The quality of the mesh at the rotor surface is improved in order to obtain proper description of skin effect.

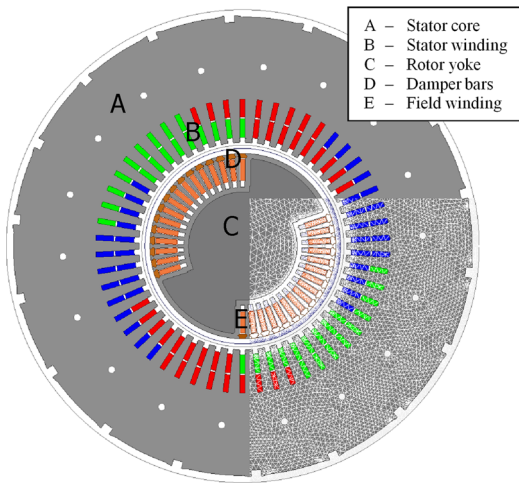


Fig. 2. Cross section of the examined turbo generator

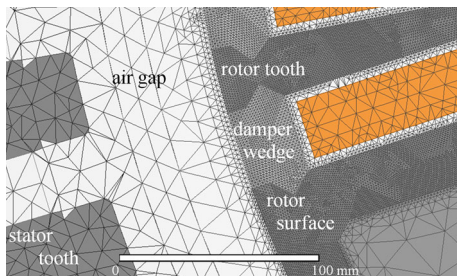


Fig. 3. Mesh of stator tooth, air gap, damper wedge and rotor yoke

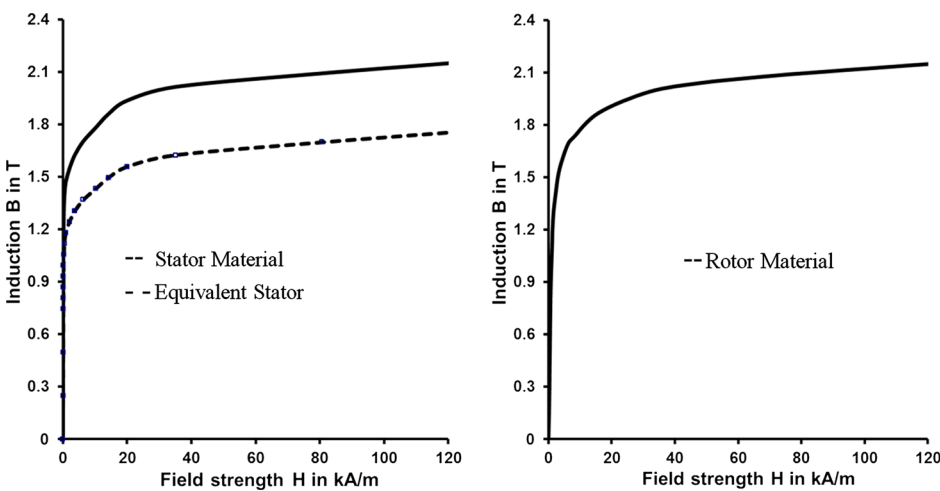


Fig. 4. Material properties of stator (left) and rotor (right)

The stator core is laminated in axial direction and has radial ventilation ducts for cooling purposes. Material properties and equivalent material properties that account for stacking factor are shown in Fig. 4; they are used for material representation in the finite element model.

The 2D model includes only the components of the straight part of the generator. The missing electric components of the 3D representation of the generator must be incorporated to the 2D finite element model. The most relevant of them is the end winding leakage reactance X_S . It is strongly affected by physical parameters of the generator components: stator end winding and rotor retaining ring. In former times the manufacturers Westinghouse and GE have used magnetic rotor retaining rings instead of non-magnetic steel ones. X_S strongly depends, whether the ring material is magnetic or not. The investigated generator is designed using non-magnetic steel retaining rings. Leakage reactance can be measured with the stator core leakage reactance test, calculated with analytical equation or 3D finite element models. Equation (3), which is derived from [4], could be used for evaluation of X_S .

$$\frac{X_S}{[\Omega]} = 0.079 \cdot \frac{f}{[50 \text{ Hz}]} \cdot \left(\frac{w}{100}\right)^2 \cdot \frac{l_S}{[\text{cm}]} \cdot \lambda_S \quad (3)$$

Here f is frequency, w is the number of stator winding turns in series for voltage induction, l_S is the length of the stator end winding and λ_S is the permeance factor. The permeance factor λ_S in Richter [8], Vogt [4], Liwschitz [6] and Bolte [7] varies, as a result the calculated leakage reactances differ from each other (see Table 1). FEA can be also used to calculate X_S . The cutting details of that 3D finite element model are shown in Fig. 5. To match the leakage reactance, which is computed with Ansys Maxwell 3D, the factor λ_S must be set to 0.328 (Table 1). The methods to evaluate X_S have been discussed in [15–17].

Figure 6 presents the equivalent external stator circuit of the 2D finite element model that accounts for the straight part main reactance X_M , armature resistance R_A and the coupled stator end turn

Table 1. Permeance factor λ_S adopted from different text books and FEA

Vogt [4]	Bolte [7]	Richter [3]	Liwschitz [6]	Current FEA
0.4	0.4828	0.2089	0.3959	0.328

leakage reactance X_S . Figure 7 shows the equivalent external rotor circuit. The circuit has a voltage source attached to the rotor terminals. Rotor end turn leakage is neglected.

The examined 2D finite element model takes into account X_H and X_f automatically. X_S , R_A , R_f and a voltage source that is added to the rotor terminals are externally connected to the model. In Sect. 5 of this manuscript the effect of modification of X_S will be discussed: half, nominal and doubled values of X_S will be applied within the FEA. This test demonstrates the robustness of the developed approach.

The investigated generator is designed with damper windings on the top of the rotor slots which are connected at the end of the rotor with the retaining ring (Fig. 8). The damper winding is also represented in the external circuit. Each damper bar is connected to the retaining ring with the wedge to retaining ring resistor. The damper winding protects the rotor winding from alternating flux penetrating during fault conditions; its effectiveness in doing so is controlled by its resistance. Larger damper resistance will lead to suppressed damper reaction and higher currents in the field winding. On the contrary smaller damper resistance will increase the damper reaction to the flux and reduce currents induced in the field winding. The finite element model accounts for damper straight part and retaining ring resistance (Fig. 9).

Since the investigated generator has 32 rotor slots, 32 wedge to retaining ring resistors are defined and connected to the mutual wedge and self-inductance L_m . Contact resistances are given in Table 2; their magnitudes depend on rotation speed, contact area, temperature and contact surface properties. When wedges are split in several pieces along the length of a rotor slot, the contact resistance of the wedge increases because of imperfect contacts between axial adjacent wedges. Market competitors use different solutions to influence these contact resistances. Two examples are presented in Figs. 10 and 11. In the first case (Fig. 10), the alignment connects each rotor wedge underneath with a solid copper bar and defined contact between axially adjacent wedges is provided. In the second case (Fig. 11) defined contact area between the wedge and the retaining ring is observed. It is covered with the silver plated

contact sheet. In Sect. 6 the effect of variation of the contact resistance will be discussed in order to demonstrate the robustness of the proposed theoretical approach.

3.2 Measurements and results of FEA

In this subsection the results of the measurements and finite element calculations at 3P-SSC are discussed.

Our model suggests that the rotation speed (50 Hz) and the winding of temperature (75 °C) remain constant. It is assumed that the

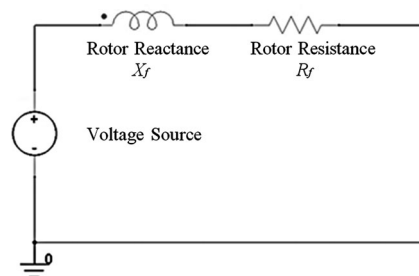


Fig. 7. External rotor circuit applied to the 2D FE Model

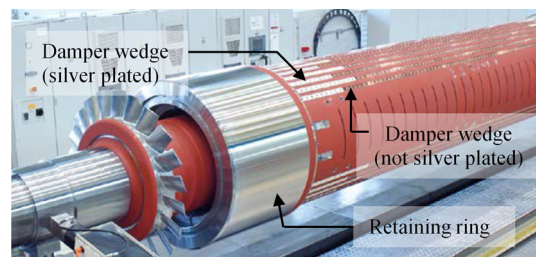


Fig. 8. SIEMENS 2-Pole Air-Cooled Generator rotor with damper winding Source: “www.energy.siemens.com/hq/pool/hq/power-generation/generators/s-gen-1200a/siemens-generators-s-gen-1200a-US-LowRes.pdf”

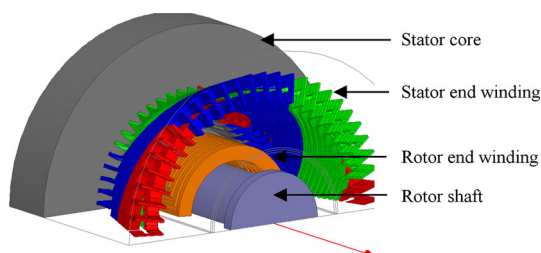


Fig. 5. 3D finite element model

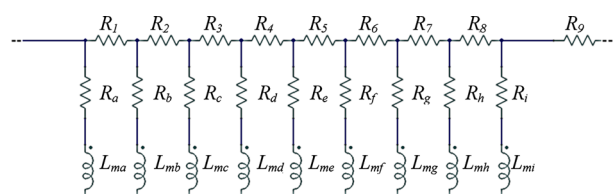


Fig. 9. Symmetric damper contact resistance—the damper circuit creates a loop of electric connected resistors and inductors

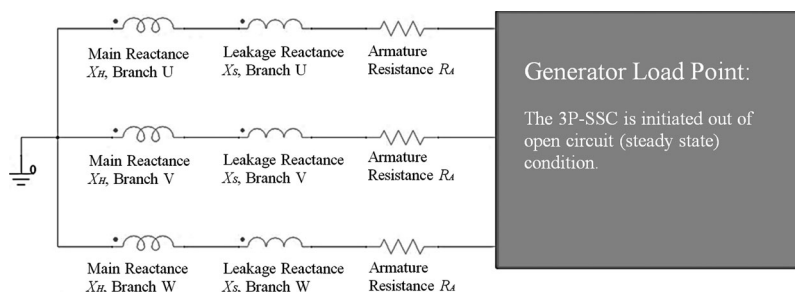


Fig. 6. External stator circuit applied to the 2D FE Model

Table 2. Contact resistors for the analyzed arrangements

Resistor	Contact	Value in mΩ
R_1, R_2, \dots	Silver plated copper—retaining ring steel	$>1.75 \times 10^{-2}$
	Not silver plated copper—retaining steel	$>2.5 \times 10^{-2}$

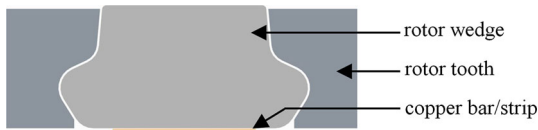


Fig. 10. Example 1—copper bars under each wedge

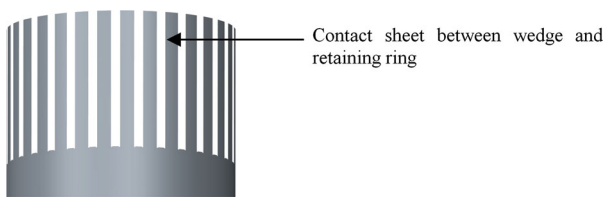


Fig. 11. Example 2—contact sheets between wedges and retaining ring

armature resistance at the 3P-SSC test is constant because of relatively large thermal time constants and short testing time. No significant temperature rise has been observed in the armature winding during the type test, which validates the assumption of constant armature resistance R_A . The resistance in the finite element model accounts not only for R_A , but also for the cables connecting the stator terminals and the shorting switch. Figures 12 and 13 show the comparison between the measured and calculated by means of FEA stator and rotor currents. The difference between theoretical and experimental results does not exceed 5 %, which validates the developed finite element model.

4. Novel approach: analysis of the field current

In this section the skin effect (eddy currents) on the rotor surface and in the damper winding will be activated and deactivated in the framework of our 2D finite element model. Such an analysis allows one to validate Eq. (2) and to develop proper theoretical formulation that accounts for damper winding and rotor surface damping. The novel equation to calculate electrical currents in field winding at 3P-SSC has the following form:

$$i_f(t) = I_{f0} \left[1 + \left(\frac{X_d}{X_d'} - 1 \right) \left(K_0 e^{-\frac{t}{T_{d0}}} + K_1 e^{-\frac{t}{T_d'}} - K_2 e^{-\frac{t}{T_d}} - K_3 e^{-\frac{t}{T_d}} \cos(\omega t) \right) \right]$$

$$K_0 = K_0(X_d'', X_d', X_d), \quad K_1 = K_1(X_d'', X_d', X_d)$$

$$K_2 = K_2(X_d'', X_d', X_d), \quad K_3 = K_3(X_d'', X_d', X_d, R_K) \quad (4)$$

Here I_{f0} is the field current before the 3P-SSC is initiated. Equation (4) contains the unknown coefficients K_0, K_1, K_2 and K_3 , which will be further referred to as K-parameters. The transient and sub-transient time constants as well as the armature time constant are kept the same as in Eq. (1). Let us comment on the newly developed Eq. (4). It describes the transient field current behavior at 3P-SSC and considers the influence of rotor surface damping and damper

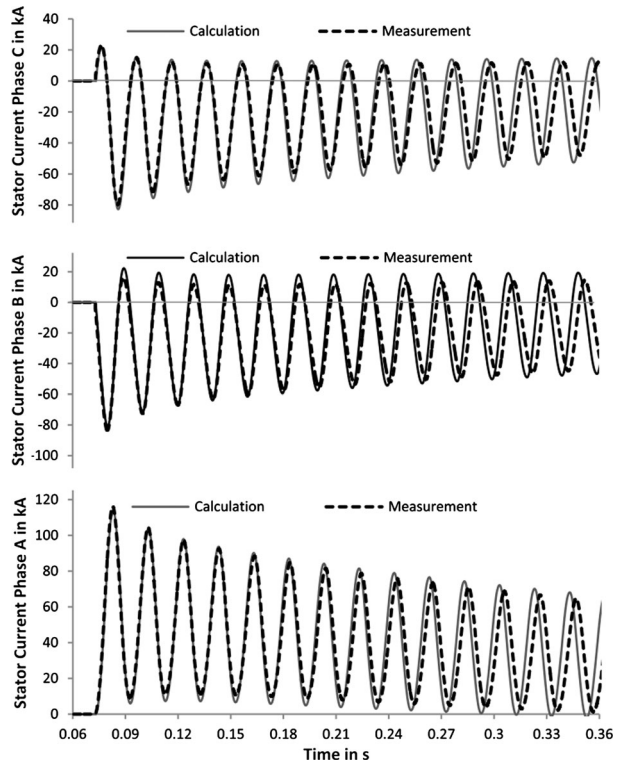


Fig. 12. Measured and calculated stator currents at 3P-SSC

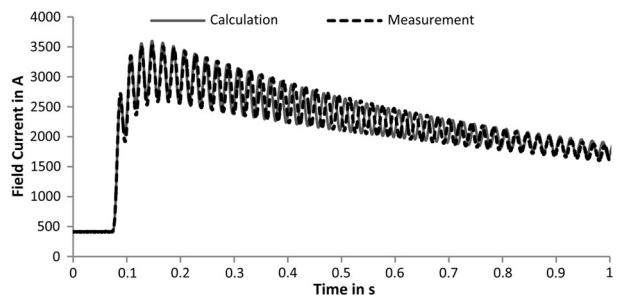


Fig. 13. Measured and calculated rotor winding current at 3P-SSC. Note: The IEC 34-3 testing allows having 15 % difference between measurements and calculation!

winding. The insert in Fig. 14 shows 4 different scenarios that are investigated with the FEA. (i) The first scenario has no damper cage and no conductive rotor surface. (ii) The second scenario has no damper cage but conductive rotor surface. (iii) The third scenario has the damper circuit but non-conductive rotor surface. (iv) In the last scenario both the rotor surface and damper circuit are conductive. Equation (4) properly describes all 4 configurations.

Each of the Figs. 15–18 includes 2 pair of indices. The first one addresses the damper circuit; the eddy effect setting can be either activated (1.ON) or not (1.OFF). The second one refers to the rotor surface, which can be either conductive (2.ON) or not (2.OFF). The currents calculated using FEA are compared with the approximation based on Eq. (4). The K-parameters are evaluated by minimization of the difference between the FEA-results and the approximated field currents.

Scenario 1: In this scenario eddy currents in the damper winding and on the rotor surface are suppressed and 3P-SSC is initiated. The field winding is strongly affected by alternating flux impinging upon

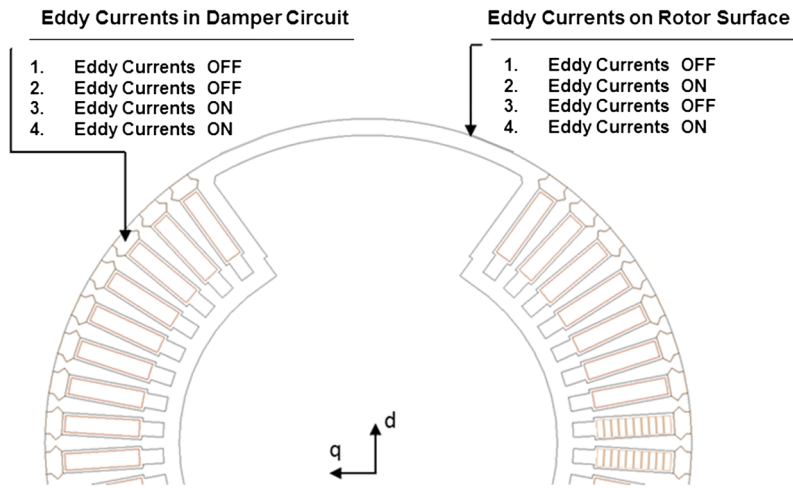


Fig. 14. Four scenarios, examined in Sect. 4

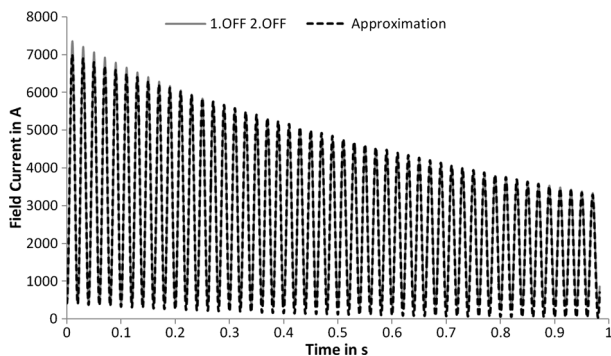


Fig. 15. Rotor winding current at 3P-SSC corresponding to scenario 1

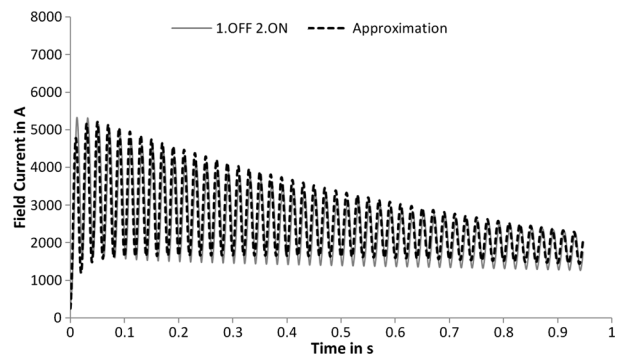


Fig. 16. Rotor winding current at 3P-SSC corresponding to scenario 2

the rotor surface. The peak magnitude of the field current equals to 7.357 kA, i.e. two times larger than the peak of 3.589 kA, shown in Fig. 13. This scenario reveals drastic increase of field current, if no eddy currents flow on the rotor surface and in the damper winding. The missing damper circuits do not protect the rotor winding from penetrating the flux. Figure 15 presents the finite element model calculation and the results of the analytical study, performed using Eq. (2). As Eq. (2) neglects sub-transient parameters, Eq. (4) is transformed into Eq. (2), if $K_0 = K_2 = 0$ and $K_1 = K_3 = 1$.

Scenario 2: In this scenario eddy currents in the damper circuit are deactivated and the damper circuit is assumed to be not conductive. The rotor surface carries eddy currents and the effect of surface damping can be studied. Figure 16 shows the results of the FEA and analytical study performed with Eq. (4). The K-parameters are listed in (5). The peak rotor current is 5.327 kA. Thus, eddy currents on the rotor surface influence the field current behavior, increasing its maximal value by 50 % with respect to the case shown in Fig. 13.

$$\begin{aligned}
 K_0 = 1 \quad K_1 = 0 \quad K_2 = 0.4 \quad K_3 = 0.6 \\
 T_{d0} = 1 \text{ s} \quad T'_d = 1.2 \text{ s} \quad T''_d = 0.0165 \text{ s} \quad T_a = 0.6 \text{ s}
 \end{aligned}
 \tag{5}$$

The rotor surface damping is represented with the coefficient K_0 , where $K_1 = 0$.

Scenario 3: In this scenario eddy currents in the damper cage are enabled but those on the steel surface of the rotor are suppressed, which can be achieved when the rotor is laminated. The interaction of the damper cage with impinging flux is in the focus of our study.

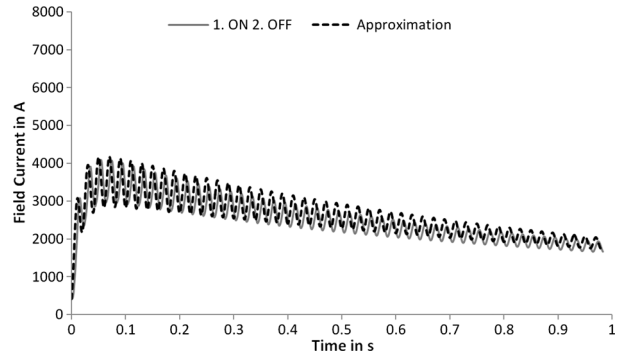


Fig. 17. Rotor winding current at 3P-SSC corresponding to scenario 3

The peak rotor current is calculated to be 4.083 kA, 114 % of that shown in Fig. 13. The results of the FEA and those obtained with Eq. (4) are presented in Fig. 17. The K-parameters are listed in (6). In this scenario K_0 is set to 0 and K_1 —to 1.

$$\begin{aligned}
 K_0 = 0 \quad K_1 = 1 \quad K_2 = 0.775 \quad K_3 = 0.225 \\
 T_{d0} = 1 \text{ s} \quad T'_d = 1.2 \text{ s} \quad T''_d = 0.0165 \text{ s} \quad T_a = 0.6 \text{ s}
 \end{aligned}
 \tag{6}$$

Scenario 4: In this scenario eddy effects are enabled on the rotor surface and in the damper bars; it corresponds to the model, which

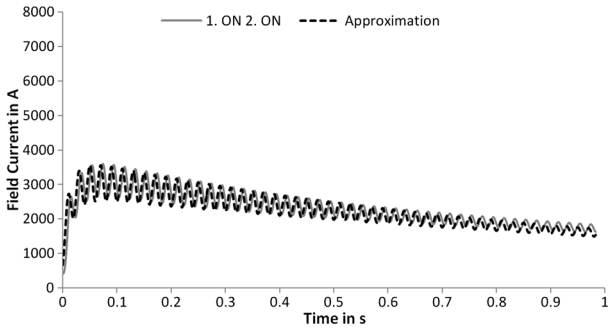


Fig. 18. Rotor winding current at 3P-SSC corresponding to scenario 4

Table 3. Summary of K-parameters for scenarios 1–4

	K-Parameters for scenarios 1–4			
	K_0	K_1	K_2	K_3
Scenario 1	0	1	0	1
Scenario 2	1	0	0.4	0.6
Scenario 3	0	1	0.775	0.225
Scenario 4	0.25	0.6	0.6	0.175

is used to generate the results from Fig. 13. This scenario exhibits the lowest rotor winding currents among four studied cases. Damper cage and rotor surface currents interact with the flux that impinges upon the rotor. The peak rotor current is 3.589 kA, i.e. the same as that in Fig. 13. The results calculated with the FEA and Eq. (4) are presented in Fig. 18. The corresponding K-parameters are listed in (7).

$$K_0 = 0.25 \quad K_1 = 0.6 \quad K_2 = 0.6 \quad K_3 = 0.175 \quad (7)$$

$$T_{dO} = 1 \text{ s} \quad T'_d = 1.2 \text{ s} \quad T''_d = 0.0165 \text{ s} \quad T_a = 0.6 \text{ s}$$

The comparison of the scenarios 1 to 4 shows that K-parameters (Eq. (4)) depend on the characteristics of rotor surface and damper bar system. They have been evaluated by means of finite element calculations by enabling and disabling conductivity of the rotor surface and the wedges. The proposed method is applicable to any generator, and the derived coefficients are unique for each considered configuration. Once they are known, the method enables series of calculations with marginal time-consumption. The FEA evaluates transient and sub-transient parameters within the accuracy of 5 % (Sect. 3). Hence the accuracy of the proposed analytical approach is the same.

The developed method is also useful for designing the rotor. Modification of the damper winding does not affect stator current behavior significantly, but influences the field winding and damper currents. The knowledge of the magnitude of the field current at 3P-SSC is essential for protecting collector sets or brushless exciter machines. The summary of all K-parameters for the scenarios 1–4 is given in Table 3.

5. Influence of the stator leakage reactance

The end turn leakage reactance X_S is one of the inputs of the finite element model studied in Sect. 3. Its value is not known exactly. The goal of this section is to reveal the effect of X_S on the stator, rotor and damper winding currents. The calculations are performed by means of Ansys Maxwell. The original value of X_S is scaled with the factors 0.5 and 2.

3P-SSC is initiated from the steady state open circuit condition. The terminal voltage as a function of time is shown in Fig. 19. Rotor

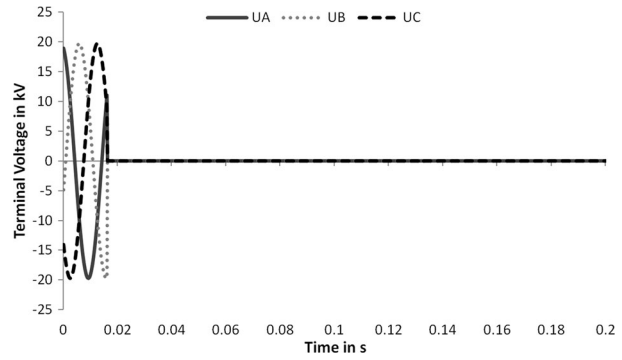


Fig. 19. Terminal voltage behavior at 3P-SSC

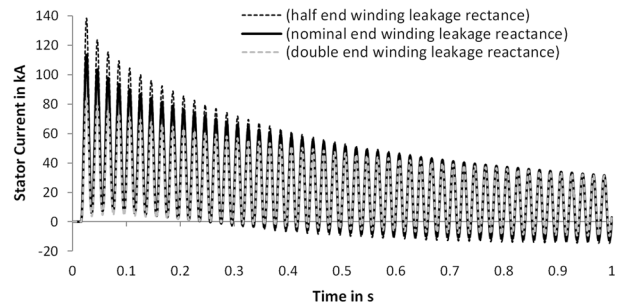


Fig. 20. Stator current at 3P-SSC for different values of X_S

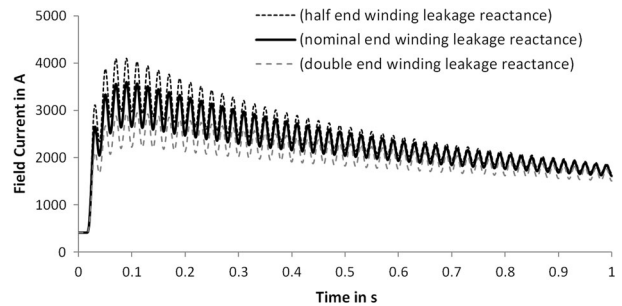


Fig. 21. Rotor winding current at 3P-SSC for different values of X_S

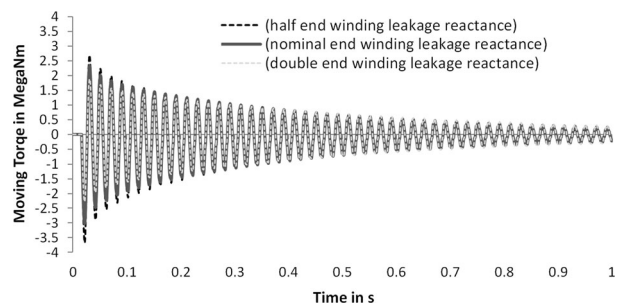


Fig. 22. Torque at 3P-SSC for different values of X_S

and stator currents rise with reduction of leakage reactance and vice versa. Figures 20 and 21 show transient rotor and stator currents at different values of X_S . The torque, presented in Fig. 22, is increased with reduction of leakage reactance as well.

The FEA gives deeper insight into the distribution of the rotor slot wedge current. Peak currents for all wedges for half, nominal and

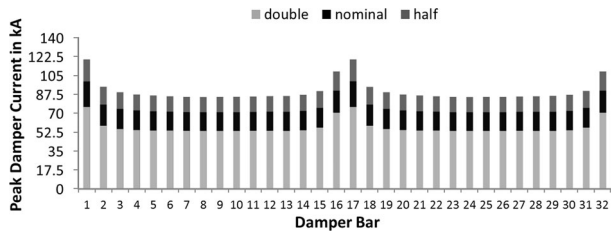


Fig. 23. Peak current distribution in rotor wedges at 3P-SSC for different X_S

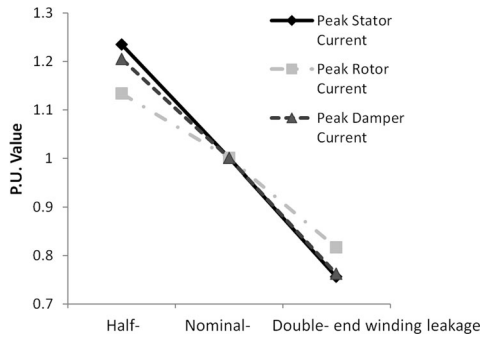


Fig. 24. Effect of X_S on the peak rotor, stator and damper currents at 3P-SSC

Table 4. K-parameters for different end winding leakage reactance X_S

X_S	Half	Nominal	Double
K_0	0.26	0.25	0.19
K_1	0.59	0.60	0.60
K_2	0.60	0.60	0.60
K_3	0.175	0.175	0.175

double magnitudes of X_S are summarized in Fig. 23. Rotor wedges that are nearest to the rotor pole edge carry highest damper currents.

Similar behavior for the stator and field winding currents could be shown analytically using Eqs. (1) and (4).

The influence of leakage reactance on the peak rotor, stator and damper bar currents is demonstrated in Fig. 24. The damper bar and the stator peak currents are proportional to each other. Moreover it has been revealed that there is almost no dependence of the K-parameters (see Table 4) upon variations of the leakage reactance. They can be influenced only when magnetic saturation changes significantly due to modification of the leakage reactance.

It is shown in [4, 6–8] and [15–17] that leakage reactance can be derived in different ways. Our investigation gives clear evidence that our method is robust with respect to variations of X_S .

6. Influence of damper winding contact resistance

In Sect. 3 it has been demonstrated that different rotor slot alignments are possible (see details Figs. 10 and 11). In this section the effect of the damper winding contact resistance on field current behavior will be examined.

The following tests reveal that the coefficient K_3 in Eq. (4) is influenced by the contact resistance $R_K = R_K(R_1, R_2, \dots)$. They are varied being scaled with the factors 1, 2 and 4. Larger damper resistance

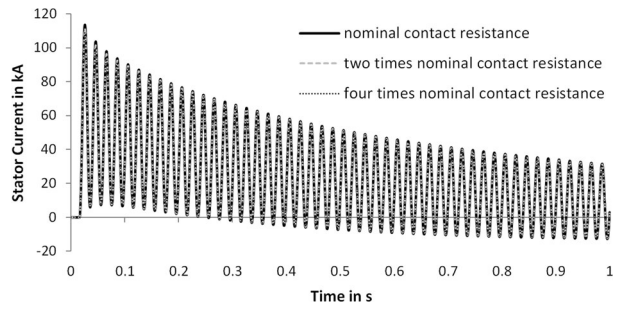


Fig. 25. Stator current at 3P-SSC for different R_K

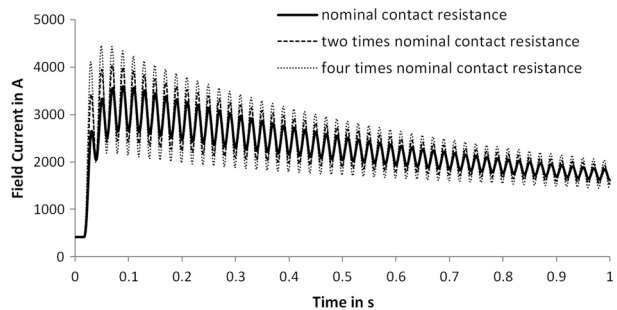


Fig. 26. Rotor winding current at 3P-SSC for different R_K

Table 5. K-Parameters for different contact resistors R_K

	Wedge to retaining ring contact resistance		
	Nominal	Double	Quadrupole
K_0	0.25	0.25	0.25
K_1	0.60	0.60	0.60
K_2	0.60	0.60	0.60
K_3	0.175	0.35	0.525

leads to suppressed reaction and higher currents in the field winding; smaller damper resistance increases the damper reaction to the flux and reduces currents induced in the field winding. The calculated stator and field winding currents for different wedge to retaining ring contacts at 3P-SSC are presented in Figs. 25 and 26. The time dependence of terminal voltage is shown in Fig. 19. The K-parameters for Eq. (4) are summarized in Table 5.

The stator current changes slightly with modification of the damper winding contact resistances, while the rotor current is affected strongly. The peak rotor current for nominal contact resistance is observed as 3.589 kA (see Sect. 3). The two times nominal contact resistance increases the peak rotor current to 4.038 kA (112.5 %), while the four times—to 4.363 kA (121.6 %).

Varying the contact resistance one affects the coefficient K_3 which is coupled to the sinusoidal part of Eq. (4). The corresponding term decays with the armature time constant.

7. Conclusion

Precise control over performance of a synchronous generator is not possible without detailed understanding of time-dependent processes associated with the currents induced in the stator and rotor windings. Our work provides the promising theoretical approach to calculate these currents at the 3P-SSC event quickly and accurately. The proposed method is a combination of the

FEA and newly developed analytical equation. First of all, the finite element model, which involves all crucial elements of a synchronous electrical machine (namely stator core and stator winding, rotor yoke and rotor winding, damper winding and conductive rotor surface), is investigated. In the second step the new analytical equation, which is based on the results of the FEA and describes the time-dependent field winding current at 3P-SSC, is presented.

Our studies have demonstrated that the developed equation is feasible for both, solid and laminated rotors, with and without damper bars. It contains 4 phenomenological coefficients for description of the time-dependent stator and rotor winding currents, which are evaluated by means of the non-linear transient finite element method. They have been identified to be unique for a given configuration of an electrical machine. The results of our theoretical approach to evaluate the transients in rotor and stator winding have been found to be in good agreement with the factory test measurements.

Acknowledgement

The author would like to thank ANSYS-Germany for sponsoring ANSYS EM Licenses for the work presented in this document. Also, the advice of Prof. Dr. Ponick of the Institute for Drive Systems and Power Electronics (IAL) Hanover has been influential in guiding this work.

References

1. Park, R. H. (1929): Two reaction theory of synchronous machines. *AIEE Trans.*, 48, 716–730.
2. Kilgore, L. (1931): The calculation of synchronous machine constants-reactances and time constants affecting transient characteristics. *AIEE Trans.*, 50, 1201–1213.
3. Concordia, C. (1951): *Theory and performance of synchronous machines*. New York: Wiley.
4. Müller, G., Vogt, K., Ponick, B. (2008): *Berechnung elektrischer Maschinen*. Weinheim: Wiley-VCH.
5. Binder, A. (2012): *Elektrische Maschinen und Antriebe*. Berlin: Springer.
6. Liwischitz, M. (1934): *Die elektrischen Maschinen: Berechnung und Bemessung* (Vol. 3). Leipzig: Teubner.
7. Bolte, E. (2012): *Elektrische Maschinen*. Berlin: Springer.
8. Richter, R. (1963): *Elektrische Maschinen: Synchronmaschinen und Einankerumformer* (Vols. 2–5, 3th ed.).
9. Canay, M. (1968): *Ersatzschemata der Synchronmaschine sowie Vorausbemessung der Kenngrößen mit Beispielen*. Dissertation, Ecole Polytechnique de l'Université de Lausanne, Lausanne
10. Wamkeue, R., Elkadr, N. E. E., Kamwa, I., Chacha, M. (2000): Unbalanced transient-based finite-element modeling of large generators. *Electr. Power Syst. Res.*, 56, 205–210.
11. Wamkeue, R., Kamwa, I., Chacha, M. (2003): Line-to-line short-circuit-based finite-element performance and parameter prediction of large hydrogen- generators. *IEEE Trans. Energy Convers.*, 18(3), 370–378.
12. Ramirez, C., Tu Xuam, M., Schafer, D., Stephan, C. (2000): Synchronous machines parameters determination using finite element method. In *International conference on electrical machines, ICEM 2000, Espoo Finland, 28–30 Aug.*, ref. 1130.
13. Schlemmer, E., Ofner, G. (2008): Finite-element investigations of the transient behavior of salient-pole synchronous machines with different damper end connections. In *Int. conf. electric machines, ICEM, Vilamoura, Portugal, 6–9 Sep.*, Paper PD.3.13.
14. Traxler-Samek, G. (2006): Computation of forces and stresses in the winding overhang of large hydrogenerators at faulty conditions. In *International conference on electrical machines, ICEM 2006*.
15. Tassarolo, A., Luise, F. (2008): An analytical-numeric method for stator end-coil leakage inductance computation in multi-phase electric machines. In *Conf. rec. IEEE IAS annu. meeting, Edmonton, Canada, 5–9 Oct.*, Paper 79.
16. Göbel, M. (2014): *Betrachtung und Berechnung magnetischer Felder im Wickelkopf 2-poliger Turbogeneratoren mit Hilfe von Ansys Maxwell*.
17. Ban, D., Zarko, D., Mandic, I. (2005): Turbogenerator end-winding leakage inductance calculation using a 3-D analytical approach based on the solution of Neumann integrals. *IEEE Trans. Energy Convers.*, 20(1), 90–105.
18. *Rotating electrical machines, part 4: Methods for determining synchronous machine quantities from tests*, IEC Std. 34-4 (1995).
19. Ranlof, M., Lundin, U. (2010): The rotating field method applied to damper loss calculation in large hydrogenerators. In *Int. conf. electric machines, ICEM, Rome, Italy, 6–9 Sep.*, Paper RF-001317.
20. Mukherjee, K., Iyer, K., Lu, X., Kar, N. (2013): A novel and fundamental approach toward field and damper circuit parameter determination of synchronous machine. *IEEE Trans. Ind. Appl.*, 49(5), 2097–2105.
21. Zhao, Z., Zheng, F., Gao, J., Xu, L. (1995): A dynamic on-line parameter identification and full-scale system experimental verification for large synchronous machines. *IEEE Trans. Energy Convers.*, 10(3), 392–398.
22. Kyriakides, E., Heydt, G., Vittal, V. (2004): On-line estimation of synchronous generator parameters using a damper current observer and a graphic user interface. *IEEE Trans. Energy Convers.*, 19(3), 499–507.
23. Bassi, C., Giulivo, D., Tassarolo, A. (2010): Transient finite-element analysis and testing of a salient-pole synchronous generator with different damper winding design solutions. In *Int. conf. electric machines, ICEM, Rome, Italy, 6–9 Sep.*, Paper RF-008079.

Author



Michael Hackbart

was born in Erfurt, Germany, in 1982. He studied electrical engineering at the TU Ilmenau where he earned the Dipl.-Ing. degree. After he had finished his studies he worked at the electrical design department at the faculty of fractional horsepower drives in Ilmenau. In 2009 he joined the SIEMENS Turbo Generator Plant in Erfurt and has been working on the development of large turbo generators.